European Journal of Medicinal Chemistry 125 (2017) 992–1001

Contents lists available at ScienceDirect

European Journal of Medicinal Chemistry

journal homepage: http://www.elsevier.com/locate/ejmech

Research paper

Chemical exploration of 4-(4-fluorobenzyl)piperidine fragment for the development of new tyrosinase inhibitors

Stefania Ferro [a, *], Laura De Luca [a], Maria Paola Germanò [a], Maria Rosa Buemi [a], Laura Ielo [a], Giovanna Certo [a, b], Margarita Kanteev [c], Ayelet Fishman [c], Antonio Rapisarda [a], Rosaria Gitto [a]

[a] Dipartimento di Scienze Chimiche, Biologiche, Farmaceutiche e Ambientali (CHIBIOFARAM) Polo Universitario SS. Annunziata, Università di Messina, Viale Annunziata I-98168 Messina, Italy
[b] Fondazione Prof. Antonio Imbesi, Piazza Pugliatti 1, 98100 Messina, Italy
[c] Department of Biotechnology and Food Engineering, Technion-Israel Institute of Technology, Haifa, 3200003, Israel

ARTICLE INFO

Article history:
Received 26 July 2016
Received in revised form
11 October 2016
Accepted 14 October 2016
Available online 18 October 2016

Keywords:
Synthesis
Tyrosinase inhibitors
SARs
Kinetic mechanism
Docking studies
Crystallography

ABSTRACT

Tyrosinase is involved in the production of melanin through the hydroxylation of monophenols to *o*-diphenols. The role of this enzyme was extensively studied in order to identify new therapeutics preventing skin pigmentation and melanoma. In this work we initially identified the 3-(4-benzylpiperidin-1-yl)-1-(1*H*-indol-3-yl)propan-1-one (**1a**) as promising mushroom tyrosinase inhibitor (IC_{50} = 252 μM). Then, several chemical modifications were performed and new analogues related to compound **1a** were synthesized. Biochemical assays demonstrated that several obtained compounds proved to be effective inhibitors showing IC_{50} values lower both than "lead compound" **1a** and reference inhibitor kojic acid, as a well-known tyrosinase inhibitor. The inhibition kinetics analyzed by Lineweaver–Burk plots revealed that compounds **2 a-c** and **10b** act as non-competitive inhibitors while the most active inhibitor **2d** (IC_{50} = 7.56 μM) is a mixed-type inhibitor. Furthermore, experimental and computational structural studies were performed in order to clarify the binding mode of the derivative **2d**.

1. Introduction

Tyrosinase (monophenol monooxygenases, EC 1.14.18.1) is a multifunctional enzyme widely distributed in nature and containing two copper ions coordinated with histidine residues in the active site. Tyrosinase is the key enzyme in the melanin biosynthesis, the main pigment commonly observed in bacteria, fungi, plants, and animals. Melanin is also responsible for human skin color [1–3]. The biosynthetic process for melanin formation occurs in two distinct reactions [4–6]. In the first two steps tyrosinase catalyzes both the hydroxylation of monophenol L-tyrosine to *o*-diphenol 3,4-dihydroxyphenylalanine (L-DOPA) (monophenolase activity) and the further oxidation of L-DOPA to *o*-quinone (diphenolase activity). Then dopaquinone, a highly reactive compound determinant in the melanogenesis, rapidly and spontaneously evolves towards the formation of various melanin pigments.

Although the melanin production shields the human skin from UV radiation, inhibiting photocarcinogenesis and affecting the synthesis of the vitamin D3 [7], an excessive accumulation of epidermal pigmentation, such us senile lentigines, freckles, ephelide, melasma and other melanin hyperpigmentation, causes serious esthetic problems in human beings [8,9].

Interestingly, it was recently demonstrated that tyrosinase is not only involved in the melanin synthesis of peripheral tissues but also in the substantia nigra (SN) of mice and humans playing a relevant role in the brain neuromelanin formation [10]. In this case, an excessive production of dopaquinones, by oxidation of dopamine, results in neuronal damage and cell death, linking tyrosinase to Parkinson's and other neurodegenerative diseases [11–13]. Thus, it extensively was highlighted the relevance of tyrosinase and there is an active interest among researchers to identify enzymatic inhibitors useful in clinical therapeutic applications as well as in cosmetic industry [14–16]. To achieve this goal different chemical classes of compounds, occurring from several sources, such as flavonoids [17–20], stilbene derivatives [21–24], kojic acid [25–29],

Abbreviations: L-DOPA, *o*-Diphenol 3,4-dihydroxyphenylalanine; SN, Substantia nigra.

* Corresponding author.
E-mail address: sferro@unime.it (S. Ferro).

http://dx.doi.org/10.1016/j.ejmech.2016.10.030
0223-5234/

tropolone [30] and novel synthetic compounds [31–38], have been investigated. Obviously, more efforts are still needed in this direction and, therefore, we recently focused our interest to this biological target.

In a previous paper [39] we have reported the serendipitous discovery of two indole derivatives (**CHI 1043** and **CHI 1164**, Fig. 1) able to inhibit the mushroom tyrosinase, displaying IC_{50} values of 224 and 372 μM, respectively.

Searching for further tyrosinase inhibitors from synthetic source, we herein describe the development of a novel series of indole derivatives in which several structural modifications were carried out. The main goal was to improve the inhibitory effects and expand our knowledge about chemical structural requirements controlling the interaction with the enzyme. Thus, the synthesized compounds were screened as mushroom tyrosinase inhibitors and their mechanism of action was explored. Moreover, experimental and computational analyses have been performed to highlight their interactions within the catalytic binding site.

2. Results and discussion

2.1. Design, synthesis and evaluation of tyrosinase inhibitory activity

In the first step of this research we selected several indole-compounds by means of a screening campaign throughout our CHIME 1.5 database, which consists of a collection of small molecules synthesized in our laboratory in the last decade. Mushroom tyrosinase has been employed for the estimation of inhibitory effects. The best effective compound was the 3-(4-benzylpiperidin-1-yl)-1-(1*H*-indol-3-yl)propan-1-one (**1a**) (Fig. 2) which proved to inhibit the diphenolase activity showing IC_{50} value of 255 μM.

Hence, we chose the active compound **1a** for generating the first series of indole analogues possessing the methoxy substituent at 5 and/or 6 position of the indole nucleus and fluorine atom on the benzyl ring (Fig. 2).

Scheme 1 summarizes the synthetic pathway employed to obtain the title compounds **1 b-d** and **2 a-d** prepared according to the previously reported method for the synthesis of "lead structure" **1a** [40].

As depicted in Scheme 1 the appropriate indole **3 a-d** was converted into the corresponding 3-acetyl derivative **4 a-d** under Vilsmeier–Haack conditions, using phosphoryl chloride and an excess of *N*,*N*-dimethylacetamide. In the next step, compounds **1 a-d** and **2 a-d** were prepared by a simple Mannich reaction between the 3-acetylindole intermediates **4 a-d**, the suitable amine derivatives and paraformaldehyde.

Inhibitory effects of indole derivatives **1 b-d** and **2 a-d** on mushroom tyrosinase activity have been evaluated and the results of the biochemical assays are summarized in Table 1. Kojic acid and 3-(4-benzylpiperidin-1-yl)-1-(1*H*-indol-3-yl)propan-1-one (**1a**) were used as reference compounds for comparative purpose.

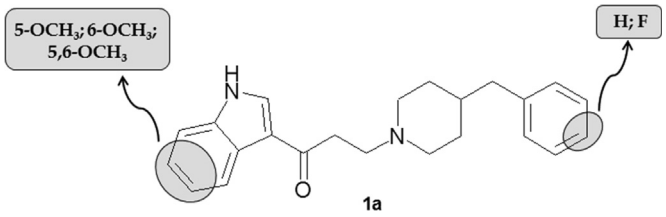

Fig. 2. The "lead compound" 3-(4-benzylpiperidin-1-yl)-1-(1*H*-indol-3-yl)propan-1-one (**1a**) retrieved from CHIME 1.5 database and the designed structural modifications.

The obtained data revealed that the first series of indole compounds **1 b-d** and **2 a-d** were effective inhibitors both of monophenolase and diphenolase activity, thus displaying IC_{50} values lower than compound **1a**. Notably derivatives **2 a-d** exhibited interesting inhibitory effect resulting more potent than kojic acid (see Table 1).

On the basis of data displayed in Table 1, the following structure-activity relationships might be drawn for this series of indole derivatives based on **1a** as lead structure.

By comparison of inhibitory effects of **1a** with the analogues **1 b-d** we can observe that the introduction of a methoxy substituent at 5- and/or 6-position of benzene fused ring generally improves the inhibitory potency toward monophenolase activity.

In addition, as depicted in Table 1 the 3-(4-benzylpiperidin-1-yl)-1-(5-methoxy-1*H*-indol-3-yl)propan-1-one (**1b**) was more potent that prototype **1a** against the two steps of melanin biosynthesis. Particularly, it was seven-fold more active than lead compound **1a** against the monophenolase activity (IC_{50} = 25.78 μM *vs* IC_{50} = 175 μM).

Furthermore, the presence of a fluorine atom at *para*-position of the benzyl moiety induces a significant improvement of activity so that the indoles **2 a-d** were up to 35-fold more potent than analogs **1 a-d** against diphenolase activity. Particularly, the most potent analogue was the 1-(5,6-dimethoxy-1*H*-indol-3-yl)-3-(4-(4-fluorobenzyl)piperidin-1-yl)propan-1-one (**2d**), in which the 5,6-dimethoxy substitution is combined with the introduction of a fluorine atom.

These data inspired us the synthesis of a further series of potential inhibitors maintaining the 3-(4-(4-fluorobenzyl)piperidin-1-yl)propan-1-one tail linked to different aromatic fragments. Pursuing the objective to explore the impact on inhibitory effects of the removal of indole nucleus of the most active compound **2d**, we planned the insertion of benzymidazole or (hetero)arylamino chemical portions. Thus, the designed *N*-substituted 3-(4-(4-fluorobenzyl)piperidin-1-yl)propanamides **7** and **10 a-c** have been synthesized as depicted in Scheme 2.

The synthesis of the 1-(1*H*-benzo[*d*]imidazol-1-yl)-3-(4-(4-fluorobenzyl)piperidin-1-yl)propan-1-one **7** (Scheme 2-A) has been carried out in two steps starting from benzimidazole **5**. By reaction with 3-chloropropionyl chloride we prepared the

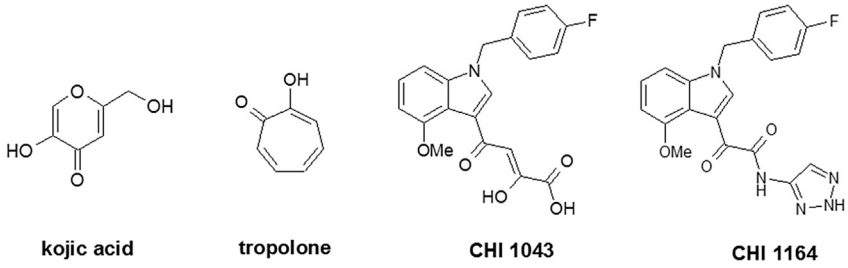

Fig. 1. Chemical structures of kojic acid, tropolone, **CHI 1043** and **CHI 1164**.

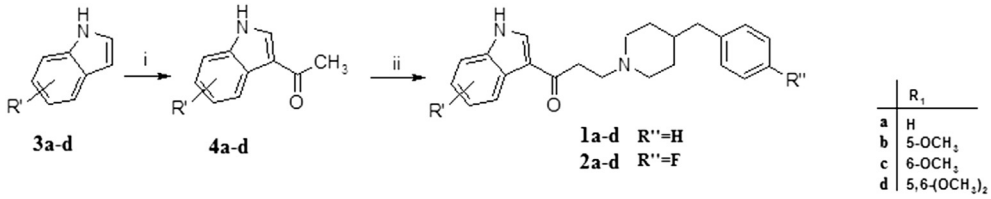

Scheme 1. Reagents and conditions: (i) $POCl_3$, *N,N*-dimethylacetamide, r.t. 24 h; (ii) DMF, paraformaldehyde, 4-benzylpiperidine hydrochloride or 4-(4-fluorobenzyl)piperidine hydrochloride, HCl 37%, MW: 3 min 80 °C.

Table 1
Inhibitory effects of indole derivatives **1 a-d**, **2 a-d** and Kojic acid on mushroom tyrosinase activity.

	Monophenolase activity IC_{50} (μM)[a]	Diphenolase activity IC_{50} (μM)[a]
1a	175.00 ± 2.71	252.00 ± 3.60
1b	25.78 ± 1.80	197.45 ± 10.62
1c	67.25 ± 5.92	168.55 ± 14.01
1d	57.24 ± 1.93	133.00 ± 2.32
2a	9.45 ± 0.36	8.82 ± 0.38
2b	7.86 ± 3.02	14.15 ± 1.60
2c	9.40 ± 0.63	18.03 ± 0.91
2d	5.11 ± 0.36	7.56 ± 1.90
Kojic acid	26.00 ± 0.13	17.76 ± 0.18

[a] All compounds were examined in a set of experiments repeated three times; IC_{50} values of compounds represent the concentration that caused 50% enzyme activity loss.

intermediate **6** which has been coupled with 4-(4-fluorobenzyl) piperidine to give the desired compound **7**. Moreover, the appropriate amine derivative **8 a-c** (Scheme 2-B) was acetylated by using 3-chloro propionyl chloride to achieve the intermediates **9 a-c**. Successively, the obtained amides **9 a-c** were treated with 4-(4-fluorobenzyl)piperidine to afford desired compounds **10 a-c**. To achieve 3-[4-(4-fluorobenzyl)piperidin-1-yl]-*N*-(1-*H*-pyrazol-3-yl) propanamide (**10c**) the amino group of the starting material 3-aminopirazole (**8c**) was opportunely protected (Scheme 2-C). Finally, the desired compound **10c** was obtained by deprotection with a mixture of DCM and TFA (see supporting data).

Next, we designed and synthesized the ketone **13** as the isostere of compound **10b** to probe the role of the NH interaction. In the first step, we prepared in good yields 3-{4-[(4-fluorophenyl)methyl] piperidin-1-yl}propanenitrile (**12**) by reaction of 4-(4-fluorobenzyl)

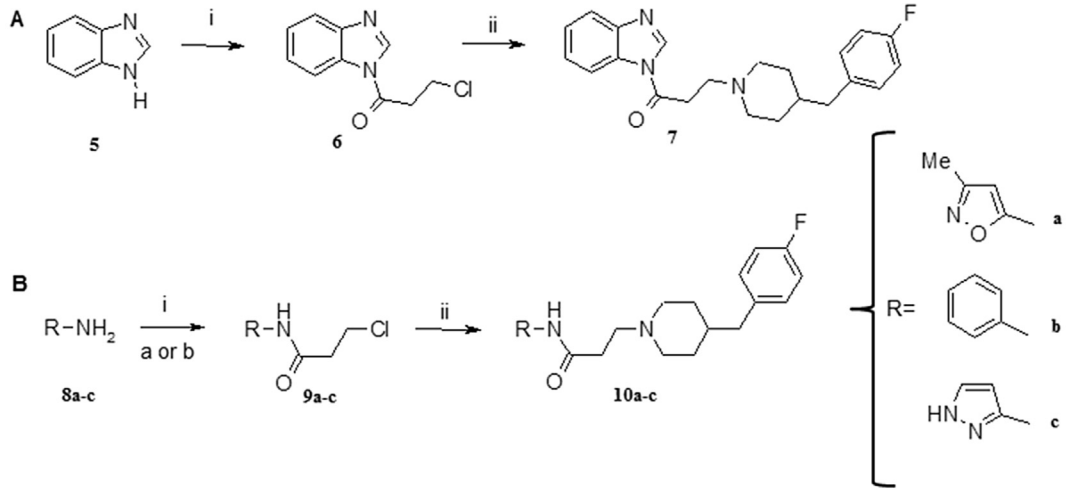

Reagents and conditions: i) (a) 3-chloro-propionyl chloride, THF, r.t 2h. ii) (b) 3-chloro-propionyl chloride, THF, K_2CO_3, r.t 16h. ii) 4-(4-fluorobenzyl)piperidine, K_2CO_3, DMF, reflux, 2h.

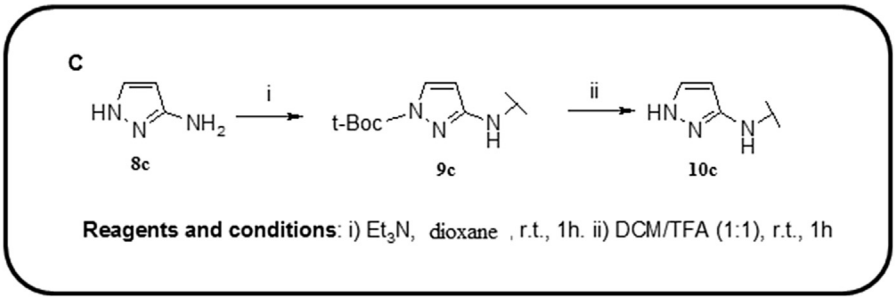

Scheme 2.

piperidine (**11**) with 3-bromopropane nitrile in alkaline medium by TEA (see Scheme 3). Then, the intermediate **12** was converted in the designed product **13** using benzyl magnesium chloride under Grignard condition.

Table 2 collects the data of the biochemical assays for the second series of designed compounds. As results the new tested compounds provided enzyme inhibitory effects at doses ranging from 27.9 to 159.24 μM. Thereby the new 4-(4-fluorobenzyl)piperidine derivatives (**7, 10 a-c, 13**) proved to be more active than prototype **1a** but they resulted less active than the corresponding indoles **2 a-d** (see Table 1). Among this new series of compounds, while the replacement of indole nucleus with phenylamine moiety (i.e. compound **10b**) or pyrazole ring (i.e. compound **10c**) produced a moderated reduction of inhibitory effects, the introduction of benzimidazole (i.e. compound **7**) or 3-methylisoxazole (i.e. compound **10a**) moiety gave a loss of activity. Overall, the most active inhibitor **10b** displayed inhibitory potency comparable to that of kojic acid (see Table 1).

By means of Gold program docking simulations were performed in attempt to draw a plausible binding mode for the most active inhibitor **2d**. Specifically, we have employed the structural coordinates (PDB code 2Y9X) of the potent inhibitor tropolone ($IC_{50} = 0.4$ μM against diphenolase activity) [41,42] in complex with the H_2L_2 tetrameric complex of mushroom tyrosinase [30].

Fig. 3 displays the docking pose of inhibitor **2d** (green) overlapping the crystal structure orientation of inhibitor tropolone (yellow) within catalytic pocket [30]. The (4-fluorobenzyl)piperidine moiety of compound **2d** is projected in a cavity forming π-π interaction with the crucial residue of His263, cation-π interaction with His244 and Van der Waals interaction with Val283. In addition, the indole nucleus of compound **2d** occupies the binding area adjacent to the entrance of the catalytic pocket cavity. The binding pose of the indole core of compound **2d** appears to be characterized by several specific contacts: a) the two oxygen atoms of the methoxy groups engage profitable hydrogen bond interactions with Asn81; b) indole NH function establishes an additional hydrogen bond contact with the carbonyl oxygen of the crucial residue His85 backbone. Finally, the proposed binding of **2d** is characterized by a lipophilic sandwich of its piperidine ring between the residues of Val248 and Val283.

Furthermore, the docking studies suggested a binding mode of the 4-fluorobenzyl portion of **2d** overlapping the inhibitor tropolone in the catalytic site of mushroom tyrosinase and sharing some key interactions. It has been reported that tropolone occupies the active site establishing van der Waals interactions with the side chain of Val283 and His263 as well as π stacking interaction with the side chain of Phe264. Furthermore, this inhibitor does not interact with the copper ions which coordinate two different set of three histidine residues (CuA: His61, His85, His94; CuB: His259, His263 and His296) [30].

Thus, to gain more information about the interactions formed by the optimized inhibitor **2d**, we choose to test the inhibitory effects of the main molecular fragments that seem to occupy two different cavities in the catalytic site of mushroom tyrosinase. Table 3 displayed the IC_{50} values determined for the four fragments: 1-(5,6-

Table 2
Inhibitory effects of derivatives **7, 10 a-c** and **13** on mushroom tyrosinase activity.

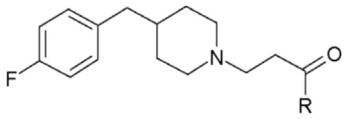

	R	Monophenolase activity IC_{50} (μM)[a]	Diphenolase activity IC_{50} (μM)[a]
7		113.34 ± 16.37	159.24 ± 18.65
10a	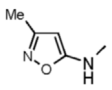	28.55 ± 0.75	110.95 ± 18.55
10b	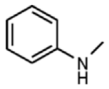	28.85 ± 0.95	27.90 ± 0.99
10c	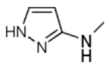	5.87 ± 1.59	39.58 ± 9.61
13		13.98 ± 0.81	83 ± 6.54

[a] All compounds were examined in a set of experiments repeated three times; IC_{50} values of compounds represent the concentration that caused 50% enzyme activity loss.

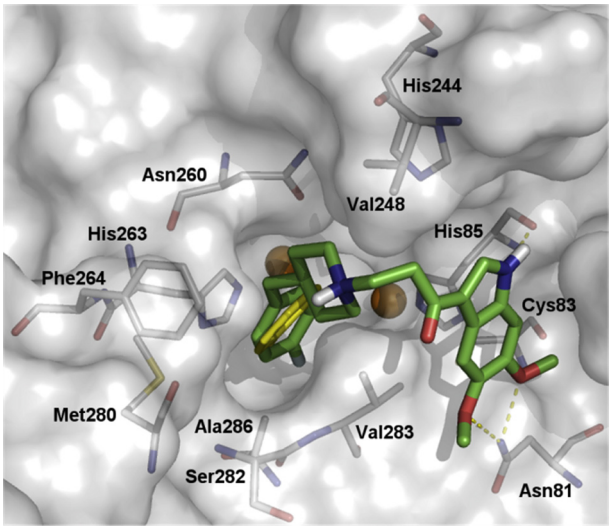

Fig. 3. Docking pose of compound **2d** (green) and **tropolone** (yellow). The copper ions are represented by orange spheres and the hydrogen bonds are drawn as yellow dashed lines. The figure was prepared in PYMOL software [54]. (For interpretation of the references to colour in this figure legend, the reader is referred to the web version of this article.)

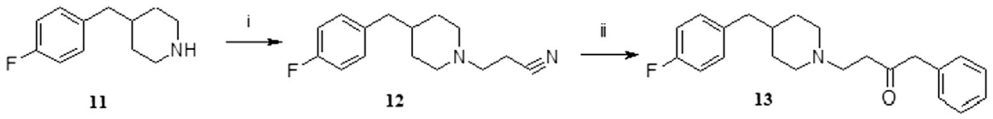

Scheme 3. Reagents and conditions: i) 3-bromopropane-nitrile, DCM, TEA, r.t., 6 h; ii) benzyl-magnesium-chloride, Et_2O, reflux, 5 h.

Table 3
Inhibitory effects of compounds **2d**, **4d, 11, 14** and **15** on mushroom tyrosinase activity.

	Monophenolase activity IC_{50} (μM)[a]	Diphenolase activity IC_{50} (μM)[a]
2d	5.11 ± 0.36	7.56 ± 1.90
4d	N.A.	N.A.
11	43.70 ± 2.61	286.83 ± 10.52
14	32.17 ± 4.19	116.0 ± 17.69
15	NA	NA

[a] All compounds were examined in a set of experiments repeated three times; IC_{50} values of compounds represent the concentration that caused 50% enzyme activity loss. NA no activity.

dimethoxy-1*H*-indol-3-yl)ethanone (**4d**), 4-(4-fluorobenzyl)piperidine **(11)** 1-ethyl-4-[(4-fluorophenyl)methyl]piperidine **(15)** and 4-[(4-fluorophenyl)methyl]-1-methylpiperidine (**16)** (See Fig. 4).

Compounds **15** and **16** were synthesized as depicted in Scheme S1 (see supporting data) following a procedures reported in literature [43,44].

It is interesting to note that the amine **11** and its *N*-ethyl derivative **(14)** inhibited tyrosinase activity (IC_{50} value of 43.7 μM and 32.17 μM respectively) in the first step of enzymatic pathway. The *N*-methyl analog **15** displays low activity when compared with ethyl and unsubstituted analogs. These experimental results were consistent with the suggested binding mode of inhibitor **2d** for which the 4-(4-fluorobenzyl)piperidine occupies the catalytic pocket of mushroom tyrosinase. By contrast, the tyrosinase activities were not absolutely affected by the indole derivative **4d**, thus suggesting that this small heterocyclic moiety occupies a binding region which is not sufficient to address inhibitory effects or that it is not able to occupy it.

2.2. Kinetic mechanism

On the basis of the mechanism of action, different classes of tyrosinase inhibitors can be distinguished: a) competitive inhibitors, which bind to the "free tyrosinase" thus preventing substrate binding; b) uncompetitive inhibitors, which bind to the tyrosinase substrate complex; c) mixed type inhibitors, which bind to not only with a free tyrosinase, but also with the tyrosinase-substrate complex, and their equilibrium binding constants for the free tyrosinase and the tyrosinase-substrate complex are different; d) non-competitive inhibitors, which could bind to a free tyrosinase and a tyrosinase-substrate complex, with the same equilibrium constant. As a consequence, to obtain further information about the type of inhibition exerted on mushroom tyrosinase by the most promising derivatives **2 a-d** and for compound **10b** the diphenolase activity was measured as a function of increasing concentration of L-DOPA and is presented using Lineweaver-Burk double reciprocal plots (see Fig. 5 and Fig. S1).

For compounds **2 a-d**, the results showed that the plots of 1/V versus 1/[S] gave straight lines with different slopes intersecting on the horizontal axis. These data suggested that compounds **2 a-c** act as non-competitive inhibitors since they are able to bind with equal affinity to the free enzyme as well as to the enzyme-substrate complex. As a consequence, the increase of **2 a-c** concentration entails the decrease of V_m value, while K_m value remains unchanged.

For **2d** derivative, a different behaviour of inhibition is observed. In fact, the Lineweaver–Burk double reciprocal plots gave straight lines with different slopes intersecting one another in the second quadrant. In this case, the reduced values of both V_m and K_m indicated that compound **2d** is a mixed-type inhibitor.

2.3. Structural studies

To further validate the predicted binding mode of compound **2d**, we carried out preliminary structural studies with TyrBm which displays 42% identity with mushroom tyrosinase.

A structure of tyrosinase from *Bacillus megaterium* (TyrBm) with bound substrates was recently reported, indicating that monophenols and diphenols bind similarly in the active site [45]. The overall structure of tyrosinases, the binding site and the catalytic mechanism are similar, although second shell residues differ among enzymes [46,47]. Obtaining crystal structures with bound ligands relies on the solubility of concentrated solutions of the desired inhibitor/substrate in the crystallization medium. Compound **2d** was soluble in DMSO, however the solvent was harmful to the TyrBm crystals. Electron density observed in the active site confirmed the presence of the inhibitor molecule (Fig. 6). A resolution of 2 Å was obtained, nevertheless, the structure was not deposited in the protein data bank since the substrate was not fully visualized.

Based on the data obtained (see supporting data), the 4-fluorobenzyl moiety of compound **2d** is situated between the two copper ions, with the aromatic ring stabilized through stacking interactions with His208 (Fig. 6B). The fluorine atom of **2d** is positioned between the copper ions, similar to the sulfur atom of phenylthiourea (PTU), in the structure of catechol oxidase from *Ipomoea batatas* (PDB code 1BUG) [48]. In this structure, the sulfur of PTU replaced the hydroxyl bridge between the copper ions. Therefore, it can be suggested that **2d** prevents oxygen binding to the active site and thus inhibits enzymatic activity. The preliminary results of the **2d** structure in complex with bacterial tyrosinase supports the positioning of the 4-fluorobenzyl moiety (Fig. 6) with

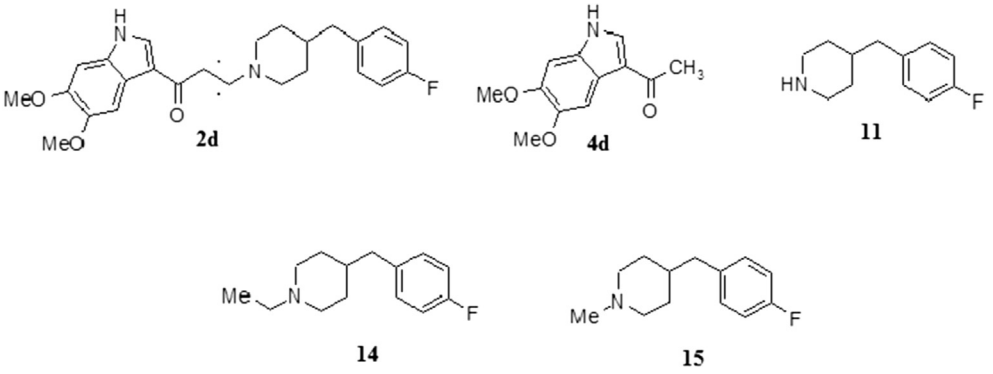

Fig. 4. Optimized inhibitor **2d** and related molecular fragments **4d, 11, 14** and **15**.

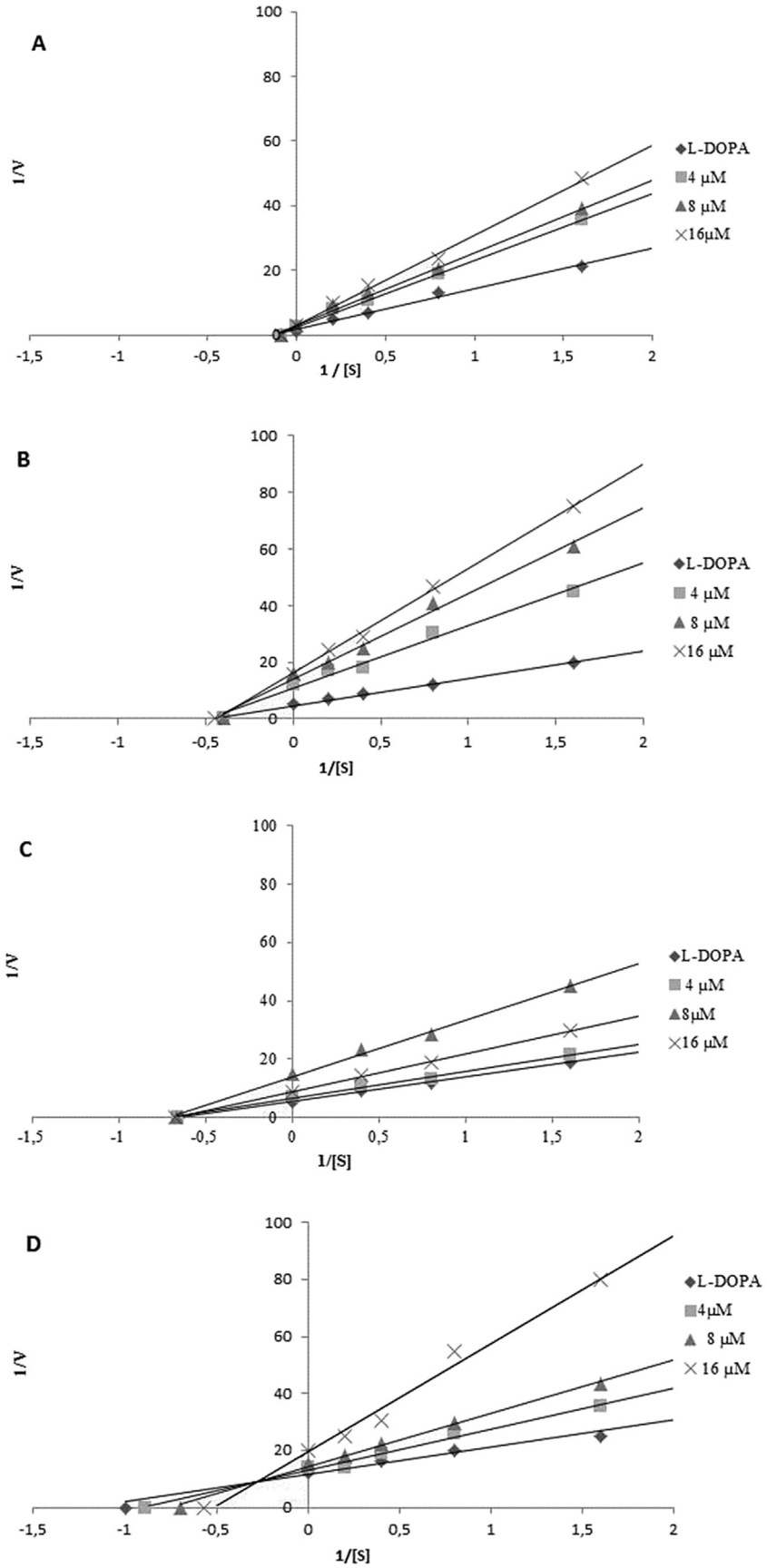

Fig. 5. Lineweaver-Burk plots for the inhibition of the diphenolase activity of mushroom tyrosinase by compounds **2a (A), 2b (B), 2c (C), 2d (D)**.

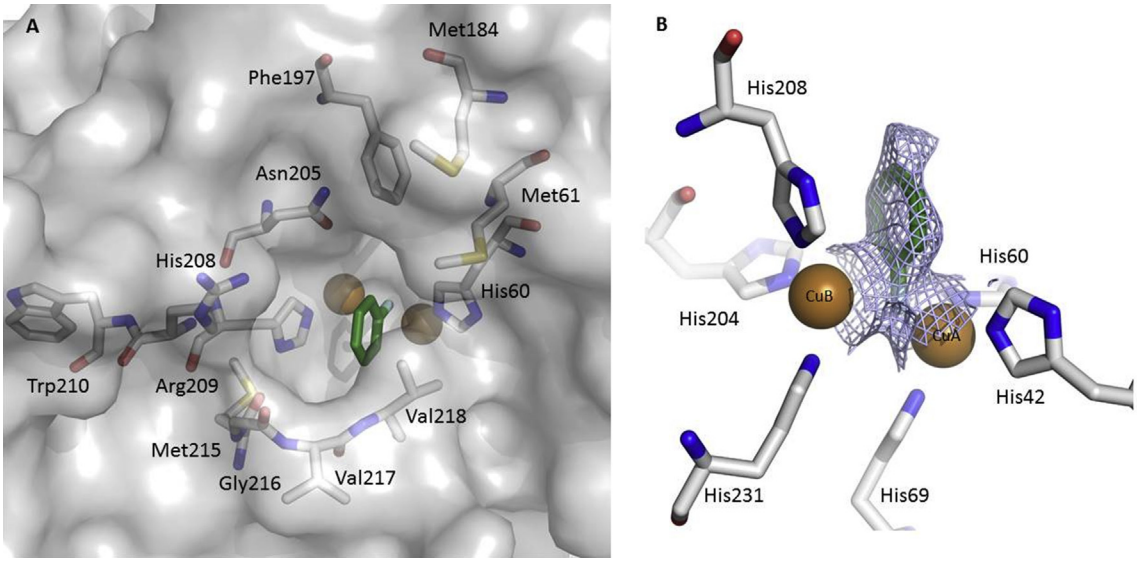

Fig. 6. Visualization of part of the molecule **2d** in the active site of tyrosinase from *Bacillus megaterium* (TyrBm). **A)** Fluorobenzene (green), the aromatic portion of **2d** is observed in the active site of TyrBm (grey surface). Copper ions are shown as brown spheres and residues surrounding the active site as white sticks. **B)** Fluorobenzene (green) with its 2Fo-Fc electron density map (light blue wire) contoured at 0.8σ. Copper ions are shown as brown spheres and histidine residues of the active site as white sticks. (For interpretation of the references to colour in this figure legend, the reader is referred to the web version of this article.)

the predicted orientation within mushroom tyrosinase (Fig. 3) for which the His263 corresponds to His208 in TyrBm.

3. Conclusions

Novel indoles as mushroom tyrosinase inhibitors have been identified. All the obtained compounds (**1 b-d, 2 a-d, 7, 10 a-c** and **13**) and the molecular fragments **11** and **14** inhibited tyrosinase at micromolar concentration. Especially, compound **2d** exhibited inhibitory activity with an IC_{50} value of 7.56 μM (diphenolase activity), higher than reference compound kojic acid. Moreover, the inhibitory mechanism and kinetics studies revealed that derivative **2d** is a mixed-type inhibitor. Finally, we compared the obtained data by means of the docking binding pose and the preliminary crystal structure of the most active compound **2d** within the catalytic pocket of mushroom tyrosinase and bacterial tyrosinase, respectively. The obtained information could aid in the design of new inhibitors. Specifically, the most interesting outcome of this study was to find that the presence of a fluorine atom on the benzyl moiety of compound **2d** exerts a significant influence on the inhibition of tyrosinase activity.

4. Experimental

4.1. Chemistry

All starting materials and reagents commercially available (Sigma-Aldrich Milan, Italy; Alfa Aesar Karlsruhe, Germany) were used without further purification. Microwave-assisted reactions were carried out in a focused Microwave Synthesis System (CEM Technology Ltd Buckingham, UK). Melting points were determined on a Buchi B-545 apparatus (BUCHI Labortechnik AG Flawil, Switzerland) and are uncorrected. Elemental analyses (C, H, N) were carried out on a Carlo Erba Model 1106 Elemental Analyzer (Carlo Erba Milano, Italy); the results confirmed a ≥95% purity. Merck silica gel 60 F254 plates were used for analytical TLC (Merck KGaA, Darmstadt, Germany). Flash Chromatography (FC) was carried out on a Biotage SP[1] EXP (Biotage AB Uppsala, Sweden). Rf values were determined on TLC plates using as eluent a mixture of DCM/MeOH (90:10) for compounds **1 b-d, 2 a-d, 7, 10 a-c**, and a mixture of DCM/MeOH (96:4) for compounds **13**, **14**, **15**. ^{1}H NMR spectra were measured in dimethylsulfoxide-d_6 (DMSO-d_6) or $CDCl_3$ with a Gemini 300 spectrometer (Varian Inc. Palo Alto, California USA); chemical shifts are expressed in δ (ppm) and coupling constants (J) in Hz.

4.1.1. General procedure for the synthesis of 1-(1H-indol-3-yl) ethanone derivatives (*4 a-d*)

Compounds **4 a-d** were prepared according a previously reported procedure [40,49]. The appropriate indole **3 a-d** (1 mmol) was added to a solution of phosphoryl chloride (0.92 mL, 10 mmol) in dimethylacetamide (2.79 mL, 30 mmol) and the resulting mixture was stirred at room temperature for 24 h. Then, the reaction mixture was basified with sodium hydroxide solution (4N) and extracted with EtOAc (3 × 10 mL). The organic phases were dried over Na_2SO_4 and the solvent removed under reduced pressure. The final compounds were obtained by crystallization with a mixture of Et_2O and DCM.

4.1.2. General procedures for the synthesis of 3-(4-benzylpiperidin-1-yl)-1-(1H-indol-3-yl)propan-1-ones (*1 a-d*, *2 a-d*)

The appropriate 3-acetyl derivative (**4 a-d**) (1 mmol) was solubilized in DMF (3 mL). Successively, paraformaldehyde (39.0 mg, 1.3 mmol), the corresponding secondary amine (4-benzylpiperidine or 4-(4-fluorobenzyl)piperidine) hydrochloride (1.1 mmol), and a catalytic amount of hydrochloric acid (37%) were added. The obtained solution was irradiated in a microwave at 80 °C for 3′ using a CEM focused Microwave Synthesis System. The mixture was quenched with H_2O and extracted with EtOAc (3 × 10 mL). The organic phases were dried with dry Na_2SO_4 and the solvent was removed in vacuo. The final compounds were obtained by purification with flash chromatography (FC, DCM/CH_3OH 90:10) and re-crystallized with Et_2O.

*4.1.2.1. 3-(4-Benzylpiperidin-1-yl)-1-(5,6-dimethoxy-1H-indol-3-yl) propan-1-one **(1d)**.* Yield: 42%, m.p. 158–160 °C; r.f. 0.20; ^{1}H NMR (DMSO-d_6) (δ) 1.26–3.08 (m, 15H), 3.87 (s, 3H, OCH_3), 3.94 (s, 3H, OCH_3), 6.86 (s, 1H, H-7), 7.14–7.30 (m, 5H, ArH), 7.69 (s, 1H, H-4),

7.88 (s, 1H, H-2), 9.48 (bs, 1H, NH). Anal. Calcd for $C_{25}H_{30}N_2O_3$: C: 73.86; H: 7.44; N: 6.89. Found: C: 73.96; H: 7.53; N: 6.87.

*4.1.2.2. 3-[4-[(4-Fluorophenyl)methyl]-1-piperidyl]-1-(1H-indol-3-yl)propan-1-one **(2a)**.* Yield 35%, m.p. 182–184 °C; r.f. 0.37; ^{1}H NMR (DMSO-d_6) (δ) 1.14–3.04 (m, 15H), 7.06–7.21 (m, 6H, ArH), 7.43 (d, 1H, $J = 8.2$), 8.16 (d, 1H, $J = 7.1$), 8.34 (s, 1H, H-2), 11.93 (bs, 1H, NH). Anal. Calcd for $C_{23}H_{25}FN_2O$: C: 75.80; H: 6.91; N: 7.69. Found: C: 75.85; H: 6.85; N: 6.72.

*4.1.2.3. 1-(5,6-Dimethoxy-1H-indol-3-yl)-2-(4-(4-fluorobenzyl) piperidin-1-yl)propan-1-one **(2d)**.* Yield 25%, m.p. 211–212 °C; r.f. 0.19; ^{1}H NMR (DMSO-d_6) (δ); 1.11–2.99 (m, 15H), 3.77 (s, 3H, OCH_3), 3.78 (s, 3H, OCH_3), 6.96 (s, 1H, H-7), 7.00–7.19 (m, 4H, ArH), 7.66 (s, 1H, H-4), 8.16 (s, 1H, H-2), 11.68 (bs, 1H, NH). Anal. Calcd for $C_{25}H_{29}FN_2O_3$: C: 70.73; H: 6.89; N: 6.60. Found: C: 70.80; H: 6.85; N: 6.65.

The spectral data for compouds **1b, 1c, 5b, 5c** are in accordance with the literature [40].

*4.1.3. General procedure for the synthesis of 1-(1-H-benzimidazol-1-yl)-3-chloropropan-1-one **(6)**, 3-chloro-N-(3-methyl-1,2-oxazol-5-yl)propanamide **(9a)** 3-chloro-N-phenyl-propanamide **(9b)** and tert-butyl-3-(3-chloropropanoylamino)pyrazole-1-carboxylate (**9c**)*

To a solution of the appropriate starting compound (**5, 8 a-c**) (1 mmol) in THF (5 mL) 3-chloro-propionyl chloride (95 μL, 1 mmol) at 0 °C and dropwise was added. For compound (**9b**) this reaction was carried out in alkaline medium by K_2CO_3 (207 mg, 1.5 mmol). The reaction mixture was stirred at room temperature for a period of 2/16 h. Successively, the reaction was quenched with $NaHCO_3$ saturated aqueous solution and extracted with EtOAc (3 × 10 mL). The organic layer was separated dried over Na_2SO_4, filtered, and concentrated under reduced pressure. The crude material was then subjected to silica gel chromatography by using cyclohexane/EtOAc (50:50).

*4.1.4. General procedure for the synthesis of 1-(1-H-benzoimidazol-1-yl)-3-(4-(4-fluorobenzyl)piperidin-1-yl)propan-1-one (**7**), 3-[4-(4-fluorobenzyl)piperidin-1-yl]-N-(3-methyl-1,2-oxazol-5-yl) propanamide (**10a**), 3-{4-[(4-Fluorophenyl)methyl]piperidin-1-yl}-N-phenylpropanamide (**10b**), and 3-[4-(4-fluorobenzyl)piperidin-1-yl]-N-(1-H-pyrazol-3-yl)propanamide (**10c**)*

4-(4-Fluorobenzyl)piperidine (1 mmol) was added to a DMF (2 mL) solution of intermediates (**6, 9 a-c**) (195 mg, 1 mmol) in alkaline medium by K_2CO_3 (276.4 mg, 2 mmol). The obtained mixture was refluxed for 2 h and then cooled at room temperature and stirred for 24 h. After this time, a $NaHCO_3$ saturated aqueous solution was added to quench the reaction and successively, the mixture was extracted with EtOAc (3 × 10 mL), dried over Na_2SO_4 and evaporated under reduced pressure. The desired compounds **7** and **10 a-c** were obtained by crystallization with Et_2O.

*4.1.4.1. 1-(1-H-Benzoimidazol-1-yl)-3-(4-(4-fluorobenzyl)piperidin-1-yl)propan-1-one **(7)**.* Yield 46%, m p. 108–110 °C; r.f. 0.34. ^{1}H NMR (DMSO-d_6) (δ): 1.07–2.89 (m, 15H), 7.02–7.50 (m, 8H, ArH), 9.58 (s, 1H, H-2). Anal. Calcd for $C_{22}H_{24}FN_3O$: C: 72.31; H: 6.62; N: 11.50. Found: C: 72.21; H: 6.42; N: 11.40.

*4.1.4.2. 3-[4-(4-Fluorobenzyl)piperidin-1-yl]-N-(3-methyl-1,2-oxazol-5-yl)propanamide (**10a**).* Yield 69%, m.p. 78–80 °C; r.f. 0.52; ^{1}H NMR (DMSO-d_6) (δ): 1.16–3.17 (m, 15H), 6.08 (s, 1H, ArH), 7.03–7.19 (m, 4H, ArH). Anal. Calcd for $C_{19}H_{24}FN_3O_2$: C: 66.07; H: 7.00; N: 12.16. Found: C: 66.27; H: 7.20; N: 12.36.

*4.1.4.3. 3-{4-[(4-Fluorophenyl)methyl]piperidin-1-yl}-N-phenyl-propanamide (**10b**).* Yield 44%, m.p. 110–112 °C; r.f. 0.40; ^{1}H NMR (DMSO-d_6) (δ): 1.14–2.89 (m, 15H), 7.00–7.09 (m, 3H, ArH), 7.15–7.17 (m, 2H, ArH), 7.26–7.29 (m, 2H, ArH), 7.52 (d, 2H, $J = 7.6$, ArH), 10.12 (bs, 1H, NH). Anal. Calcd for $C_{21}H_{25}FN_2O$: C: 74.09; H: 7.40; N: 8.23. Found: C: 74.29; H: 7.60; N: 8.43.

*4.1.4.4. 3-[4-(4-Fluorobenzyl)piperidin-1-yl]-N-(1-H-pyrazol-3-yl) propanamide (**10c**).* Yield 64%, m.p. 137–139 °C; r.f. 0.05; ^{1}H NMR (DMSO-d_6) (δ): 1.21–2.95 (m, 15H), 6.44 (s, 1H, ArH), 7.07–7.20 (m, 8H, ArH), 7.55 (s, 1H, ArH), 10.55 (bs, 1H, NH). Anal. Calcd for $C_{18}H_{23}FN_4O$: C: 65.43; H: 7.02; N: 16.96. Found: C: 65.53; H: 7.12; N: 16.86.

*4.1.5. Synthesis of 3-{4-[(4-fluorophenyl)methyl]piperidin-1-yl} propanenitrile (**12**)*

To a stirred solution of 4-(4-fluorobenzyl)piperidine **(11)** (400 mg, 2.1 mmol) in CH_2Cl_2 (4.7 mL) was added 3-bromopropane-nitrile (281 mg, 2.1 mmol) and TEA (0.6 mL, 4.2 mmol). The mixture was stirred at room temperature for 6 h and after TLC analysis, using as eluent DCM/MeOH 96:4, was added H_2O (5 mL) and the solution was extracted with CH_2Cl_2 (3 × 5 ml). The organic phase was dried over Na_2SO_4 and the solvent removed under reduced pressure to give the final compound as a yellow oil.

*4.1.6. Synthesis of 3-[4-(4-fluorobenzyl)piperidin-1-yl]-1-phenyl-4-butan-2-one (**13**)*

To a mixture of benzyl-magnesium-chloride in Et_2O (1 M) (2.4 mL, 2.4 mml) was added a solution of intermediate **12** (303 mg, 1.2 mmol) in Et_2O (1 mL). The reaction mixture was heated at reflux for 2 h. After a TLC analysis, using as eluent DCM/MeOH 96:4, was added a saturated ammonium chloride solution. The mixture was extracted with Et_2O. The organic phase was dried over Na_2SO_4 and the solvent removed under reduced pressure to give the final compound as a yellow oil residue. Yield 92%, oil, r.f. 0.68; ^{1}H NMR ($CDCl_3$) 1.22–1.33 (m, 2H, 2CH), 1.50 (m, 1H, CH), 1.59–1.64 (m, 2H, 2CH), 1.95–2.02 (m, 2H, 2CH), 2.45–2.50 (m, 4H, $2CH_2$), 2.63–2.67 (m, 2H, CH_2), 2.84–2.87 (m, 2H, CH_2), 4.68 (s, 2H, CH_2), 6.92–6.98 (m, 2H, ArH), 7.07–7.10 (m, 2H, ArH), 7.17–7.37 (m, 3H, ArH). Anal. Calcd for $C_{22}H_{26}FNO$: C: 77.84; H: 7.72; N: 4.13. Found: C: 78.24; H: 8.12; N: 4.53.

4.2. Mushroom tyrosinase inhibition assay

Tyrosinase inhibition was assayed according to the method of Masamoto [50] with minor modifications [51]. Briefly, aliquots (0.05 mL) of sample at various concentrations (5–300 μM) were mixed with 0.5 mL of L-tyrosine or L-DOPA solution (1.25 mM), 0.9 mL of sodium acetate buffer solution (0.05 M, pH 6.8) and preincubated at 25 °C for 10 min. Then 0.05 mL of an aqueous solution of mushroom tyrosinase (333 U/mL) was added last to the mixture. The linear increase in adsorbance (Abs) at 475 nm was measured after 30 or 5 min of incubation time in the reaction mixture containing L-tyrosine or L-DOPA, respectively. The inhibitory activity of samples is expressed as inhibition percentage and calculated as follows:

$$\text{Inhibition } \% = \{[(A-B)-(C-D)]/A-B\}/100.$$

A: Abs acetate buffer and enzyme.
B: Abs acetate buffer.
C: Abs acetate buffer, test sample and enzyme.
D: Abs acetate buffer and test sample.

The concentrations leading to 50% activity lost (IC_{50}) were also calculated by interpolation of the dose-response curves. Kojic acid [5-hydroxy-2-(hydroxymethyl)-4*H*-pyran-4-one], a fungal secondary metabolite used as skin whitening agent, was employed as a positive standard (8–35 μM).

4.3. Kinetic analysis of the tyrosinase inhibition

The inhibition kinetics of the most active compounds on the tyrosinase were studied using Lineweaver–Burk double reciprocal plots [52]. For the test, the reaction mixture consisted of four different concentrations of L-DOPA (0.6–5 mM) as substrate and mushroom tyrosinase in acetate buffer (0.05 M, pH 6.8). Test samples at various concentrations (4–16 μM) were added to the reaction mixture.

4.4. Docking analysis

The crystal structure of Agaricus Bisporus Mushroom Tyrosinase in complex with inhibitor tropolone was retrieved from the RCSB Protein Data Bank (PDB code 2Y9X). The ligand and water molecules were discarded and the hydrogens were added to the protein by Discovery Studio 2.5 [53].

The ligand structure was constructed using Discovery Studio 2.5.5 and energy minimized using the Smart Minimizer protocol (1000 steps) which combines the Steepest Descent and the Conjugate Gradient methods. The minimized ligand was docked in their corresponding proteins by means of Gold Suite 5.0.1. The region of interest used by the Gold program was defined in order to contain the residues within 15 Å from the original position of the ligand in the X-ray structure. GoldScore was chosen as fitness function. The standard default settings were used in all calculations and the ligands were submitted to 100 genetic algorithm runs. The "allow early termination" command was deactivated. Results differing by less than 0.75 Å in ligand-all atom RMSD, were clustered together. The highest GOLD fitness score was chosen both for analysis and representation. The molecular model of the docked compound was displayed using Pymol software [54].

4.5. Crystallization and data collection

TyrBm crystals were prepared as described [45]. Crystallization drops containing TyrBm crystals were supplemented with 1 μl solution of 5 mM in 25% PEG 8K and 1 μl of 50 mM **2d** in 100% DMSO. It should be noted that only a small fraction of **2d** was dissolved in DMSO. After overnight incubation, most of the crystals were destroyed or damaged due to the presence of DMSO. Several crystals which were not destroyed were frozen in liquid nitrogen. X-ray diffraction data was collected at the European Synchrotron Radiation Facility (ESRF), Grenoble, France, at beamline ID29. The diffraction data was indexed, integrated, and reduced with Mosflm and Scala [55]. The structure was solved by Phaser-MR using PDB code 3NM8 as initial model [56]. Manual model building, real-space refinement, and structure validations were performed using Coot [57]. Partial structure statistics are presented in Table S1 (see supporting data). A resolution of 2 Å was obtained, nevertheless, the structure was not deposited in the protein data bank since the substrate was not fully observed.

Acknowledgements

This research was supported by Fondo di Ateneo per la Ricerca University of Messina (ORME09SPNC). The authors are thankful to the Israel Science Foundation founded by the Israel Academy of Sciences and Humanities, grant number 419/15 for financial support. We thank the staff of the European Synchrotron Radiation Facility (beamline ID 29) for provision of synchrotron radiation facilities and assistance.

Appendix A. Supplementary data

Supplementary data related to this chapter can be found at http://dx.doi.org/10.1016/j.ejmech.2016.10.030.

References

[1] E.I. Solomon, U.M. Sundaram, T.E. Machonkin, Multicopper oxidases and oxygenases, Chem. Rev. 96 (1996) 2563–2606.
[2] M. Shiino, Y. Watanabe, K. Umezawa, Synthesis of N-substituted N-nitrosohydroxylamines as inhibitors of mushroom tyrosinase, Bioorg. Med. Chem. 9 (2001) 1233–1240.
[3] X.H. Huang, Q.X. Chen, M.S. You, Q. Wang, K.K. Song, J. Wang, L. Sha, X. Guan, Inhibitory effects of fluorobenzaldehydes on the activity of mushroom tyrosinase, J. Enzyme Inhib. Med. Chem. 21 (2006) 413–418.
[4] H.S. Raper, The anaerobic oxidases, Physiol. Rev. 8 (1928) 245–282.
[5] H.S. Mason, The chemistry of melanin; mechanism of the oxidation of dihydroxyphenylalanine by tyrosinase, J. Biol. Chem. 172 (1948) 83–99.
[6] A.B. Lerner, T.B. Fitzpatrick, et al., Mammalian tyrosinase; preparation and properties, J. Biol. Chem. 178 (1949) 185–195.
[7] N.G. Lindquist, Accumulation of drugs on melanin, Acta Radiol. Diagn. (Stockh) 325 (1973) 1–92.
[8] F. Solano, S. Briganti, M. Picardo, G. Ghanem, Hypopigmenting agents: an updated review on biological, chemical and clinical aspects, Pigment. Cell Res. 19 (2006) 550–571.
[9] S. Briganti, E. Camera, M. Picardo, Chemical and instrumental approaches to treat hyperpigmentation, Pigment. Cell Res. 16 (2003) 101–110.
[10] T. Pan, X. Li, J. Jankovic, The association between Parkinson's disease and melanoma, Int. J. Cancer 128 (2011) 2251–2260.
[11] M. Asanuma, I. Miyazaki, N. Ogawa, Dopamine- or L-DOPA-induced neurotoxicity: the role of dopamine quinone formation and tyrosinase in a model of Parkinson's disease, Neurotox. Res. 5 (2003) 165–176.
[12] Z.H. Zhu, YJ, Y.H. Hu, J.Y. Tang, M.X. Su, Y.J. Guo, L.B. Chen, QX, Antityrosinase and antimicrobial activities of 2-phenylethanol, 2-phenylacetaldehyde and 2-phenylacetic acid, Food Chem. 124 (2011) 298–302.
[13] Y. Xu, A.H. Stokes, R. Roskoski Jr., K.E. Vrana, Dopamine, in the presence of tyrosinase, covalently modifies and inactivates tyrosine hydroxylase, J. Neurosci. Res. 54 (1998) 691–697.
[14] J. Choi, S.J. Park, J.G. Jee, Analogues of ethionamide, a drug used for multidrug-resistant tuberculosis, exhibit potent inhibition of tyrosinase, Eur. J. Med. Chem. 106 (2015) 157–166.
[15] Z. Ashraf, M. Rafiq, S.Y. Seo, K.S. Kwon, M.M. Babar, N.U. Zaidi, Kinetic and in silico studies of novel hydroxy-based thymol analogues as inhibitors of mushroom tyrosinase, Eur. J. Med. Chem. 98 (2015) 203–211.
[16] A. You, J. Zhou, S. Song, G. Zhu, H. Song, W. Yi, Structure-based modification of 3-/4-aminoacetophenones giving a profound change of activity on tyrosinase: from potent activators to highly efficient inhibitors, Eur. J. Med. Chem. 93 (2015) 255–262.
[17] I. Kubo, I. Kinst-Hori, S.K. Chaudhuri, Y. Kubo, Y. Sanchez, T. Ogura, Flavonols from Heterotheca inuloides: tyrosinase inhibitory activity and structural criteria, Bioorg. Med. Chem. 8 (2000) 1749–1755.
[18] L.P. Xie, Q.X. Chen, H. Huang, H.Z. Wang, R.Q. Zhang, Inhibitory effects of some flavonoids on the activity of mushroom tyrosinase, Biochem. (Mosc) 68 (2003) 487–491.
[19] J.K. No, D.Y. Soung, Y.J. Kim, K.H. Shim, Y.S. Jun, S.H. Rhee, T. Yokozawa, H.Y. Chung, Inhibition of tyrosinase by green tea components, Life Sci. 65 (1999) PL241–246.
[20] Y.J. Kim, Rhamnetin attenuates melanogenesis by suppressing oxidative stress and pro-inflammatory mediators, Biol. Pharm. Bull. 36 (2013) 1341–1347.
[21] B.B. Aggarwal, A. Bhardwaj, R.S. Aggarwal, N.P. Seeram, S. Shishodia, Y. Takada, Role of resveratrol in prevention and therapy of cancer: preclinical and clinical studies, Anticancer Res. 24 (2004) 2783–2840.
[22] N.H. Shin, S.Y. Ryu, E.J. Choi, S.H. Kang, I.M. Chang, K.R. Min, Y. Kim, Oxyresveratrol as the potent inhibitor on dopa oxidase activity of mushroom tyrosinase, Biochem. Biophys. Res. Commun. 243 (1998) 801–803.
[23] K. Shimizu, R. Kondo, K. Sakai, S.H. Lee, H. Sato, The inhibitory components from Artocarpus incisus on melanin biosynthesis, Planta Med. 64 (1998) 408–412.
[24] K. Likhitwitayawuid, B. Sritularak, A new dimeric stilbene with tyrosinase inhibitiory activity from Artocarpus gomezianus, J. Nat. Prod. 64 (2001) 1457–1459.
[25] G.A. Burdock, M.G. Soni, I.G. Carabin, Evaluation of health aspects of kojic acid in food, Regul. Toxicol. Pharmacol. 33 (2001) 80–101.
[26] R. Bentley, From miso, sake and shoyu to cosmetics: a century of science for kojic acid, Nat. Prod. Rep. 23 (2006) 1046–1062.
[27] A.F. Lajis, M. Hamid, A.B. Ariff, Depigmenting effect of Kojic acid esters in hyperpigmented B16F1 melanoma cells, J. Biomed. Biotechnol. 2012 (2012)

952452.
[28] J.J. Molenda, M.A. Basinger, T.P. Hanusa, M.M. Jones, Synthesis and iron(III) binding properties of 3-hydroxypyrid-4-ones derived from kojic acid, J. Inorg. Biochem. 55 (1994) 131–146.
[29] H. Kim, J. Choi, J.K. Cho, S.Y. Kim, Y.S. Lee, Solid-phase synthesis of kojic acid-tripeptides and their tyrosinase inhibitory activity, storage stability, and toxicity, Bioorg. Med. Chem. Lett. 14 (2004) 2843–2846.
[30] W.T. Ismaya, H.J. Rozeboom, A. Weijn, J.J. Mes, F. Fusetti, H.J. Wichers, B.W. Dijkstra, Crystal structure of Agaricus bisporus mushroom tyrosinase: identity of the tetramer subunits and interaction with tropolone, Biochemistry 50 (2011) 5477–5486.
[31] M.R.T. Loizzo, R. Tundis, F. Menichini, Natural and synthetic tyrosinase inhibitors as antibrowning agents: an update, Compr. Rev. Food Sci. Food Saf. 11 (2012) 378–398.
[32] Y.J. Kim, H. Uyama, Tyrosinase inhibitors from natural and synthetic sources: structure, inhibition mechanism and perspective for the future, Cell Mol. Life Sci. 62 (2005) 1707–1723.
[33] N. Gencer, D. Demir, F. Sonmez, M. Kucukislamoglu, New saccharin derivatives as tyrosinase inhibitors, Bioorg. Med. Chem. 20 (2012) 2811–2821.
[34] Y.K. Han, Y.J. Park, Y.M. Ha, D. Park, J.Y. Lee, N. Lee, J.H. Yoon, H.R. Moon, H.Y. Chung, Characterization of a novel tyrosinase inhibitor, (2RS,4R)-2-(2,4-dihydroxyphenyl)thiazolidine-4-carboxylic acid (MHY384), Biochim. Biophys. Acta 1820 (2012) 542–549.
[35] J.W. Park, Y.M. Ha, K.M. Moon, S.R. Kim, H.O. Jeong, Y.J. Park, H.J. Lee, J.Y. Park, Y.M. Song, P. Chun, Y. Byun, H.R. Moon, H.Y. Chung, De novo tyrosinase inhibitor: 4-(6,7-dihydro-5H-indeno[5,6-d]thiazol-2-yl)benzene-1,3-diol (MHY1556), Bioorg. Med. Chem. Lett. 23 (2013) 4172–4176.
[36] H. Hamidian, R. Tagizadeh, S. Fozooni, V. Abbasalipour, A. Taheri, M. Namjou, Synthesis of novel azo compounds containing 5(4H)-oxazolone ring as potent tyrosinase inhibitors, Bioorg. Med. Chem. 21 (2013) 2088–2092.
[37] Z. Zhou, J. Zhuo, S. Yan, L. Ma, Design and synthesis of 3,5-diaryl-4,5-dihydro-1H-pyrazoles as new tyrosinase inhibitors, Bioorg. Med. Chem. 21 (2013) 2156–2162.
[38] K.W. Lam, A. Syahida, Z. Ul-Haq, M.B. Abdul Rahman, N.H. Lajis, Synthesis and biological activity of oxadiazole and triazolothiadiazole derivatives as tyrosinase inhibitors, Bioorg. Med. Chem. Lett. 20 (2010) 3755–3759.
[39] S. Ferro, G. Certo, L. De Luca, M.P. Germano, A. Rapisarda, R. Gitto, Searching for indole derivatives as potential mushroom tyrosinase inhibitors, J. Enzyme Inhib. Med. Chem. 31 (2016) 398–403.
[40] M.R. Buemi, L. De Luca, S. Ferro, R. Gitto, Targeting GluN2B-containing N-Methyl-D-aspartate receptors: design, synthesis, and binding affinity evaluation of novel 3-substituted indoles, Arch. Pharm. (Weinheim) 347 (2014) 533–539.
[41] K. Lida, K. Hase, K. Shimomura, S. Sudo, S. Kadota, T. Namba, Potent inhibitors of tyrosinase activity and melanin biosynthesis from rheum officinale, Planta Medica 61 (1995) 425–428.
[42] W. Kahn, A. Andrawis, Inhibition of mushroom tyrosinase by tropolone, Phytochemistry 24 (1985) 905–908.
[43] J.L. Herndon, A. Ismaiel, S.P. Ingher, M. Teitler, R.A. Glennon, Ketanserin analogues: structure-affinity relationships for 5-HT2 and 5-HT1C serotonin receptor binding, J. Med. Chem. 35 (1992) 4903–4910.
[44] C. Abate, S. Ferorelli, M. Contino, R. Marottoli, N.A. Colabufo, R. Perrone, F. Berardi, Arylamides hybrids of two high-affinity sigma2 receptor ligands as tools for the development of PET radiotracers, Eur. J. Med. Chem. 46 (2011) 4733–4741.
[45] M. Goldfeder, M. Kanteev, S. Isaschar-Ovdat, N. Adir, A. Fishman, Determination of tyrosinase substrate-binding modes reveals mechanistic differences between type-3 copper proteins, Nat. Commun. 5 (2014) 4505.
[46] M. Kanteev, M. Goldfeder, A. Fishman, Structure-function correlations in tyrosinases, Protein Sci. 24 (2015) 1360–1369.
[47] C.A. Ramsden, P.A. Riley, Tyrosinase: the four oxidation states of the active site and their relevance to enzymatic activation, oxidation and inactivation, Bioorg. Med. Chem. 22 (2014) 2388–2395.
[48] T. Klabunde, C. Eicken, J.C. Sacchettini, B. Krebs, Crystal structure of a plant catechol oxidase containing a dicopper center, Nat. Struct. Biol. 5 (1998) 1084–1090.
[49] R. Gitto, L. De Luca, S. Ferro, E. Russo, G. De Sarro, M. Chisari, L. Ciranna, J. Alvarez-Builla, R. Alajarin, M.R. Buemi, A. Chimirri, Synthesis, modelling and biological characterization of 3-substituted-1H-indoles as ligands of GluN2B-containing N-methyl-d-aspartate receptors, Bioorg. Med. Chem. 22 (2014) 1040–1048.
[50] Y. Masamoto, H. Ando, Y. Murata, Y. Shimoishi, M. Tada, K. Takahata, Mushroom tyrosinase inhibitory activity of esculetin isolated from seeds of Euphorbia lathyris L, Biosci. Biotechnol. Biochem. 67 (2003) 631–634.
[51] M.P. Germano, F. Cacciola, P. Donato, P. Dugo, G. Certo, V. D'Angelo, L. Mondello, A. Rapisarda, Betula pendula leaves: polyphenolic characterization and potential innovative use in skin whitening products, Fitoterapia 83 (2012) 877–882.
[52] K.F. Huang, Y.W. Chen, C. Chang, S.T. Chou, Studies on the inhibitory effect of Graptopetalum paraguayense E. Walther extracts on mushroom tyrosinase, Food Chem. 89 (2005) 583–587.
[53] Accelrys, Discovery Studio.
[54] http://www.pymol.org.
[55] A. Leslie, Joint CCP4 and ESF-EACMB, Newsletter on Protein Crystallography, Daresbury Laboratory, Warrington, UK, 1992, p. 26.
[56] A.J. McCoy, Solving structures of protein complexes by molecular replacement with Phaser, Acta Crystallogr. D. Biol. Crystallogr. 63 (2007) 32–41.
[57] P. Emsley, K. Cowtan, Coot: model-building tools for molecular graphics, Acta Crystallogr. D. Biol. Crystallogr. 60 (2004) 2126–2132.